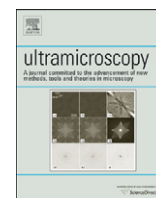




ELSEVIER

Contents lists available at ScienceDirect

## Ultramicroscopy

journal homepage: [www.elsevier.com/locate/ultramic](http://www.elsevier.com/locate/ultramic)

# A systematic procedure for determining the chiral indices of multi-walled carbon nanotubes using electron diffraction—each and every shell

Hakan Deniz<sup>a</sup>, Anna Derbakova<sup>a</sup>, Lu-Chang Qin<sup>a,b,\*</sup>

<sup>a</sup> Department of Physics and Astronomy, University of North Carolina at Chapel Hill, Chapel Hill, NC 27599-3255, USA

<sup>b</sup> Curriculum in Applied Sciences and Engineering, University of North Carolina at Chapel Hill, Chapel Hill, NC 27599-3255, USA

## ARTICLE INFO

## Article history:

Received 6 August 2009

Received in revised form

27 August 2010

Accepted 29 September 2010

## Keywords:

Electron diffraction

Carbon nanotubes

## ABSTRACT

Electron diffraction technique has been developed and refined to establish a systematic procedure to determine the chirality (chiral indices) of each and every shell in a carbon nanotube. We have introduced a zoning scheme to sort the reflection layer lines from the multiple shells of a carbon nanotube. An application of the procedure is demonstrated as an example for an eleven-shell carbon nanotube whose chiral indices of each and every shell were determined unambiguously. The revealed structure of the carbon nanotube suggests that there is no strong correlation among the shells as the nanotube was formed. The limitations of the current method are also discussed.

© 2010 Elsevier B.V. All rights reserved.

## 1. Introduction

Carbon nanotubes (CNTs) are a novel form of carbon with unique structures and fascinating properties [1]. The electronic properties of a carbon nanotube are highly sensitive to its atomic structure, which is well described by a pair of integers  $(u, v)$  known as the chiral indices that define the perimeter vector (chiral vector) of the nanotube by  $\vec{C}_{uv} = u\vec{a}_1 + v\vec{a}_2$ , in which  $\vec{a}_1$  and  $\vec{a}_2$  are the basis vectors of the graphene lattice with an inter-angle of  $60^\circ$ . For example, a carbon nanotube is metallic if  $(u - v) = 3q$  ( $q$  is an integer), otherwise it is semi-conducting [2,3]. A single-walled carbon nanotube (SWNT) is formed by rolling up a graphene into a cylindrical structure about an axis perpendicular to its chiral vector  $\vec{C}_{uv}$ . Therefore, the helicity and the diameter of a nanotube are also dictated by its chiral indices  $(u, v)$ . The helicity  $\alpha = \arctan[\sqrt{3}v/(v + 2u)]$  of a carbon nanotube of chiral indices  $(u, v)$  is defined as the angle between the chiral vector  $\vec{C}_{uv}$  and basis vector  $\vec{a}_1$  of the graphene lattice, and its diameter  $d$  is given by  $d = a\sqrt{u^2 + v^2 + uv}/\pi$  where  $a = 0.2461$  nm is the lattice constant of graphene. So, any slight change in the value of  $u$  or  $v$  can drastically alter the atomic structure and the electronic properties of a carbon nanotube. This shows the necessity and importance of complete and unambiguous determination of the chiral indices  $(u, v)$  of a carbon nanotube for both understanding of the structure-property relationships and envisaged future applications of carbon nanotubes in nanotechnology.

\* Corresponding author at: Department of Physics and Astronomy, University of North Carolina at Chapel Hill, Chapel Hill, NC 27599-3255, USA.  
E-mail address: [lcqin@physics.unc.edu](mailto:lcqin@physics.unc.edu) (L.-C. Qin).

Several optical spectroscopic methods have been developed and applied to obtain the chiral indices of carbon nanotubes, such as resonant Raman spectroscopy (RRS), photoluminescence, and optical absorption spectroscopy [4–8]. In RRS, the chiral indices are assigned by combining the information from inter-band transition energies with the phonon frequencies. The radial breathing mode (RBM) in Raman spectroscopy is also sensitive to the diameter of carbon nanotubes but it is only effective for the nanotubes of small diameter  $d$  ( $d < 2$  nm). In addition, resonant Raman spectroscopy also requires a broad range of laser wavelengths to study nanotubes of various chiralities. Photoluminescence which is a process of absorption and emission of photons between the ground and excited states can be used to reveal the electronic structure and in turn to determine the chiral indices of CNTs. Its main drawback is that it only works for semi-conducting carbon nanotubes. Absorption spectroscopy is another means to probe the electronic states by looking at the characteristic absorption wavelengths. It can detect both metallic and semi-conducting nanotubes. However, it is limited by inadequate spatial resolution of the measurements and the effect of the tubule-environment interactions on transition energies.

Non-optical methods include scanning tunneling microscopy (STM), high-resolution transmission electron microscope (HRTEM) imaging in the real space, and electron diffraction in the reciprocal space [9–31]. By direct imaging in the real space, the diameter  $d$  and the helicity  $\alpha$  of a carbon nanotube are measured first to assign the chiral indices when atomic images are obtained using high performance transmission electron microscopes equipped with aberration-correctors. However, in HRTEM imaging, high-quality images with atomic resolution are difficult to obtain due to instabilities, lens aberrations, focusing, etc. that often complicate the interpretation of the recorded images. Its successes have only

been limited to SWNTs. On the other hand, STM not only can resolve the electronic structure, but also can identify the atomic structure at the same time. Unfortunately, it is only useful at best for the identification of the helicity of the outermost shell in multi-walled carbon nanotubes (MWNTs) with limited spatial resolution in the measurement of diameter.

Electron diffraction has been the most popular and powerful method to study the atomic structure of carbon nanotubes with a high accuracy since their discovery [11]. Electron diffraction patterns (EDPs) of carbon nanotubes are not subject to such adverse effects like instabilities or lens aberrations as much as the real-space images are. Nano-beam electron diffraction technique has exhibited great successes in obtaining the chiral indices of individual SWNTs [25,26]. A one-step direct method involving accurate expressions of the scattering intensities using Bessel functions on the reflection layer lines has been recently developed to retrieve the chiral indices of SWNTs [25]. Since the peak positions of a Bessel function of particular order are unique, the order of the Bessel function can be obtained by measuring the ratio of first two peak positions from the intensity oscillations on a concerned layer line. With this method, the indices  $(u,v)$  can be determined directly from the electron diffraction pattern. This method has been demonstrated to work for determining the chiral indices in the range up to (30,30) and the accuracy is limited by the experimental capability in differentiating adjacent Bessel functions of large orders.

In this paper, we present a systematic procedure using electron diffraction to obtain the chiral indices  $(u,v)$  of each and every shell of multi-walled carbon nanotubes and the method is applied, as an example, to obtain the chiral indices of all shells of an eleven-shell carbon nanotube.

## 2. Zoning scheme

A MWNT can be regarded as a collection of SWNTs nested with one another concentrically and its electron diffraction pattern can be explained in terms of a sum of the electron diffraction pattern of each SWNT constituting the MWNT. The electron diffraction pattern from a SWNT can be considered as a superposition of two sets of hexagonal reflections that are resulted from the “top” and the “bottom” graphene layer of the nanotube, respectively. However, the reflections from a SWNT and those from graphene show striking differences in appearance because of the finite size of the nanotube in the radial direction and its cylindrical curvature. The reflections from a SWNT are elongated in the direction normal to the tubule axis and exhibit themselves as a set of equally spaced layer lines due to the well-defined periodicity of the nanotube in the axial direction. Fig. 1 shows a simulated electron diffraction pattern of carbon nanotube with chiral indices (18,3). Three pairs of principal layer lines, formed by the primary Bragg reflections, are seen in the EDP. The major reflections from the honeycomb lattice of graphene in the reciprocal space are twisted relative to each other by a twist angle that is closely related to the helicity of the carbon nanotube. These lines are labeled as  $L_1$ ,  $L_2$  and  $L_3$  in descending order with spacings  $D_1$ ,  $D_2$  and  $D_3$ , respectively. Another striking feature of the electron diffraction patterns of carbon nanotubes is that the reflections of a SWNT always show 2 mm symmetry regardless if the structure of the nanotubes itself has such symmetry [32].

On each principal layer line, the scattering intensity is modulated by the square of a sum of Bessel functions of different orders but is dominated by a single Bessel function of the lowest order  $|J_n(\pi R d)|^2$ , where  $R$  is the radial distance measured along the layer line from the tubule axis in the reciprocal space [32]. For a SWNT of chiral indices  $(u,v)$ , the three principal layer lines,  $L_1$ ,  $L_2$  and  $L_3$ , are formed by

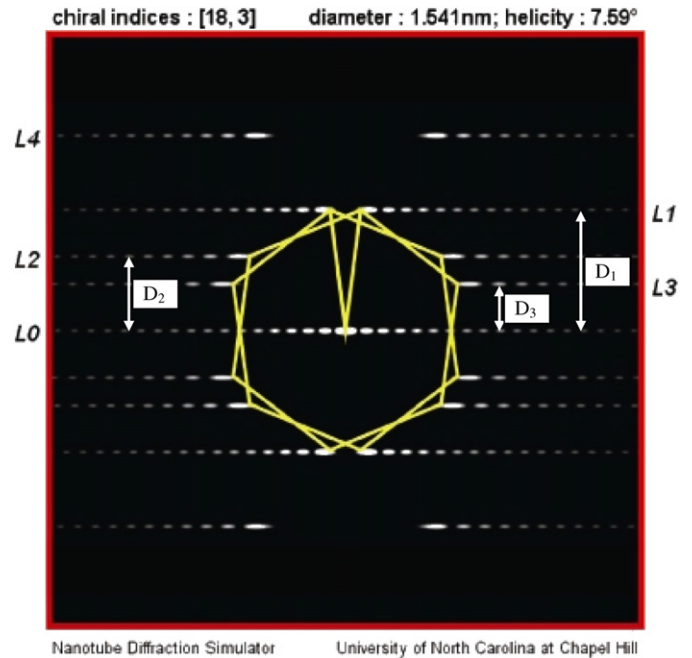


**Fig. 1.** Simulated electron diffraction pattern of carbon nanotube of chiral indices (18,3) with normal incidence. The two hexagons mark the primary reflections of graphene with which the three principal layer lines  $L_1$ ,  $L_2$  and  $L_3$  are formed with the layer line spacings  $D_1$ ,  $D_2$  and  $D_3$ , respectively. The higher order reflection labeled as  $L_4$  is also visible in the square frame.

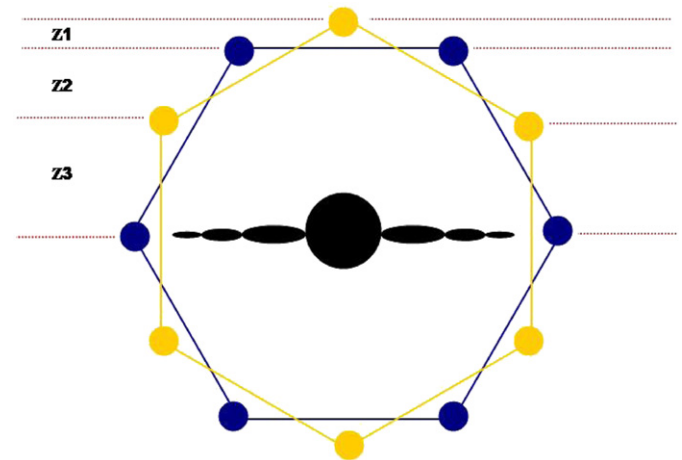


**Fig. 2.** Schematic drawing of the reflections of armchair and zigzag nanotubes in reciprocal space together with three zones ( $Z_1$ ,  $Z_2$  and  $Z_3$ ) defined by these reflection layer lines. For a chiral carbon nanotube, the three principal layer lines  $L_1$ ,  $L_2$  and  $L_3$  will lie within their respective zones  $Z_1$ ,  $Z_2$  and  $Z_3$ .

graphene reflections  $(0\ 1)$ ,  $(\bar{1}\ 0)$  and  $(1\ 1)$ , respectively. The order  $n$  of the dominating Bessel function on a given graphene reflection  $(h\ k)$  is obtained through the following relation [17]:

$$n = hu + kv \quad (1)$$

If we choose graphene reflection  $(0\ 1)$  that forms the principal layer line  $L_1$ , where  $h=0$  and  $k=1$ , the order of the concerned Bessel function is  $n=v$ . For the principal layer lines  $L_2$  and  $L_3$  that are formed by graphene reflections  $(\bar{1}\ 0)$  and  $(1\ 1)$ , respectively, the corresponding order  $n$  is  $n=-u$  for layer line  $L_2$  and  $n=u+v$  for layer line  $L_3$ . On the equatorial layer line, the scattering intensity is

proportional to the square of Bessel function of order zero, i.e.,  $|J_0(\pi R d)|^2$ .

We can divide the reciprocal space into three zones, designated by  $Z_1$ ,  $Z_2$  and  $Z_3$ , as illustrated schematically in Fig. 2 that contain the three principal layer lines,  $L_1$ ,  $L_2$  and  $L_3$ , in the reciprocal space. In the axial direction, they are expressed by  $Z_1$ :  $[1/a, 2/(\sqrt{3}a)]$ ;  $Z_2$ :  $[1/(\sqrt{3}a), 1/a]$  and  $Z_3$ :  $[0, 1/(\sqrt{3}a)]$ ; where  $a=0.2461$  nm is the lattice constant of graphene. In terms of the factor  $1/a$ , the three zones are then  $Z_1$ :  $[1, 1.154]$ ;  $Z_2$ :  $[0.577, 1.0]$  and  $Z_3$ :  $[0, 0.577]$ .

With the zoning scheme defined above, regardless of the chiral indices  $(u, v)$  of each shell, the first principal layer line  $L_1$  will always be in zone  $Z_1$ , the second principal layer line  $L_2$  will always be in zone  $Z_2$  and  $L_3$  will always be in  $Z_3$ . Within each zone, the layer lines from different shells will be arranged in an ordered sequence. The  $L_1$  and  $L_3$  lines will be in descending order as the helicity increases, while the  $L_2$  lines will be in ascending order.

This zoning scheme is very helpful to sort the layer lines in terms of the originating shells. For an  $N$ -shell carbon nanotube, if there is no degeneracy in helicity, there will be  $N$  layer lines in each of the three zones. The first line in zone  $Z_1$ , the last line in zone  $Z_2$  and the first line in zone  $Z_3$  will be from the same shell that has the smallest helicity. The second line in zone  $Z_1$ , the second last line in zone  $Z_2$  and the second line in zone  $Z_3$  will be from the same shell of the second smallest helicity. In general, the  $n^{\text{th}}$  line from the top in zone  $Z_1$ , the  $n^{\text{th}}$  line from the bottom in zone  $Z_2$  and the  $n^{\text{th}}$  line from the top in zone  $Z_3$  are from the same shell.

In the case of achiral nanotubes (zigzag or armchair nanotubes), there is no twist angle between the reflections from top and bottom layers. Here the orientation of hexagonal honeycomb lattice with respect to the tubule axis determines the value of the helical angle. The helicity of  $0^\circ$  corresponds to zigzag tubes whereas the helicity of  $30^\circ$  is to armchair nanotubes. In the EDP of achiral nanotubes, the layer lines  $L_1$  and  $L_2$  are coincident and the  $L_3$  layer line falls on the equator for armchair nanotubes while the layer lines  $L_2$  and  $L_3$  coincide with each other for zigzag nanotubes. For a zigzag nanotube, the layer line  $L_1$  lies farthest away from the equator whereas it is closest to the equator for an armchair nanotube.

It should be noted that the principal layer lines are not evenly dispersed in the three zones as the three zones have different widths:  $\Delta Z_1=0.154/a$ ,  $\Delta Z_2=0.423/a$  and  $\Delta Z_3=0.577/a$ . They are more dispersed in zone  $Z_3$  than in zones  $Z_1$  and  $Z_2$ .

### 3. Methods

Here, we measure the layer line spacings from the experimental EDPs to identify all helical angles and to obtain the ratio of the chiral indices for each shell. The ratio of  $v$  to  $u$  can be expressed as [24]

$$\frac{v}{u} = \frac{2D_2 - D_1}{2D_1 - D_2} \quad (2)$$

This ratio can be obtained with a high accuracy since the layer lines are sharp owing to the axial periodicity of the nanotube. It is also independent of the incident angle of the electron beam and the camera length at which the EDP was taken. The direct method for obtaining the chiral indices  $(u, v)$  of a carbon nanotube using the Bessel functions can be applied as a complementary check when possible. Other complementary information that can aid the indexing of MWNTs is the break-down of the 2 mm symmetry on a principal layer line, which is an indicator for the case of coherent interferences of the electron waves from two different shells of the same helicity but their chiral indices have opposite evenness/oddity [32].

Since the electron diffraction pattern of a chiral nanotube manifests three pairs of principal layer lines, for a MWNT of  $N$  shells with each having a different helicity, we would expect to see

$3N$  pairs of layer lines in its electron diffraction pattern. This means that there should be  $N$  layer lines in the first zone,  $N$  layer lines in the second one and  $N$  layer lines in the third zone. If one helicity is repeated, we will see  $3N - 3$  pairs of layer lines in total and  $N - 1$  layer lines in each zone. For the shells of close helicities, some principal layer lines might appear overlapped in the diffraction pattern due to experimental limitations and this will make the number of layer lines in each zone uneven. In this case, the relationship  $D_1 = D_2 + D_3$  can be used as a complementary equation to group the layer lines into their respective helicities. In general, the procedure for determination of the chiral indices of a multi-walled carbon nanotube, assuming that all shells are chiral, can be broken down into the following steps:

1. Acquire electron diffraction patterns and HREM images. Check the number of principal layer lines in the electron diffraction pattern and the number of graphene shells in the nanotube. If the number of principal layer lines is three times the number of shells, each shell will have a different helicity and each zone in the diffraction pattern has the same number of layer lines. If one or more helicities are repeated, the number of principal layer lines in each zone will not be equal to the number of shells but there is still the same number of layer lines in each zone.
2. Measure the layer line spacings of the principal layer lines as accurately as possible from the acquired electron diffraction pattern. Also obtain the number of shells and their approximate diameters from the HRTEM images.
3. Group the principal layer lines for each helicity starting with the smallest one. The smallest helicity means that layer line  $L_1$  is positioned farthest away from the equator (nanotube of zigzag structure being the smallest). As the helicity increases, the  $L_1$  and  $L_2$  layer lines move towards each other and the  $L_3$  layer line moves toward the equator. The set of layer lines with the smallest helicity can be obtained by picking the first layer line from zone  $Z_1$ , the last one from zone  $Z_2$  and the first one again from zone  $Z_3$ . The set with the next smallest helicity can be obtained in a similar way: picking the second layer line in zone  $Z_1$ , the second last in zone  $Z_2$  and the second one in zone  $Z_3$ . In this way all layer lines can be identified with each helicity without use of any complementary equations.
4. When two layer lines are too close to each other and cannot be resolved very well due to experimental limitations, they might appear as one layer line. Obviously this will make the number of layer lines in each zone uneven. The equation  $D_1 = D_2 + D_3$  can then be used to identify each helicity by keeping in mind that a layer line cannot belong to two different zones or two different helicities.
5. Once all helicities are identified and the principal layer lines from the same helicity are matched, the ratio of chiral indices ( $v/u$ ) is calculated using equation (2). The uncertainty in the measured  $v/u$  ratio can be calculated through equation (2) by error propagation using the errors in the measurement of layer line spacings.
6. Find all possible chiral indices satisfying the measured  $v/u$  ratios within the experimental uncertainties and matching the measured diameters approximately.
7. If a layer line is due to only one shell in the nanotube, the direct method can be used to retrieve the order of Bessel function by analysis of intensity oscillations if the order of Bessel function in question is not very high.
8. Use the characteristic (0 0 2) spacing of graphite ( $d_{200} \sim 0.34$  nm) as a constraint to obtain the inter-shell distances as reasonable as possible with the index assignment. Start with the assignment of tubules of smaller diameters since there are fewer possibilities for the chiral indices of smaller nanotubes. If some helicities are

repeated in the structure, it will limit the choice of chiral indices to an integer multiple of the smallest ones possible for that repeating helicity. If there is a break-down of the 2 mm symmetry in intensities on a layer line with respect to the tubule axis for a helicity repeated twice, opposite evenness/oddness of the possible chiral indices for that helical set can be used to pick the best index assignment.

9. Check the index assignment by comparing the simulated intensity of the equatorial layer line with the experimental intensity to improve accuracy. If they fail to match each other closely, repeat the assignment procedure until the simulated intensity agrees with the experimental one for each possible index assignment.

In the case that the MWNT under investigation has armchair/zigzag shells or both, there will not be equal number of principal layer lines in each zone. However, these two structures can be easily identified from the layer lines using their unique intensity distributions. For example, for a zigzag nanotube, the intensity of layer line  $L_1$  is governed by the Bessel function of zero-th order and a strong single diffraction spot in the first zone in the axial direction will be observed. The same is true and applicable for the intensity of high order layer line  $L_4$  with an armchair nanotube.

#### 4. An example of application

A high-resolution electron microscope image and an electron diffraction pattern of an eleven-shell carbon nanotube taken at an accelerating voltage of 120 kV, which is below the threshold of knock-on radiation damage for graphene (139 kV) [34], are shown in Figs. 3 and 4, respectively. For this eleven-shell carbon nanotube, the inter-shell spacing between the innermost and outermost shell is taken to be ten times of the average (0 0 2) spacing of graphite ( $d_{002}=0.34$  nm) and this length is used as the scale to measure the diameter of each shell. The electron microscope (JEM-2010F) was operated in a nano-beam mode to produce a fine electron beam of 20–30 nm in diameter for acquisition of the diffraction patterns. Total 23 layer lines in the first-order reflections were identified from the diffraction pattern and their layer line spacings were measured several times to reduce round-off errors in the measurements. There were no reflections corresponding to zigzag or armchair nanotubes in the diffraction patterns. Eight distinct helicities were identified from a grouping of the 23 layer lines (see Table 1)—one “missing” principal layer line in overlap with another in zone  $Z_1$ . The first layer line in zone  $Z_1$  is formed by two layer lines spaced too closely with respect to one another to be

resolved experimentally although they belong to two different helicities. This can also be obtained using the complementary relationship  $D_1=D_2+D_3$  and any small difference can be used as an experimental error to estimate the uncertainty in the  $v/u$  ratios through a simple error propagation equation. We therefore have seven layer lines in zone  $Z_1$ , eight layer lines in zone  $Z_2$  and eight layer lines in zone  $Z_3$ , while the first layer line in the zone  $Z_1$  belongs to two close helicities. The layer lines from all the three zones are grouped according to their respective helicities by starting with the

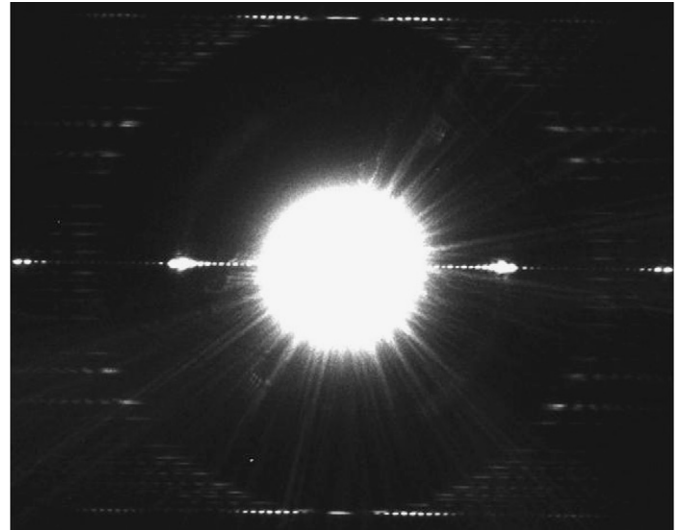


Fig. 4. Nano-beam electron diffraction pattern of the eleven-shell carbon nanotube shown in Fig. 3.

Table 1

Experimentally measured layer line spacings (in arbitrary unit)  $D_1$ ,  $D_2$  and  $D_3$ , uncertainty in layer line spacings  $\sigma_D$ , index ratio  $v/u$  and their propagated errors for the eleven-shell carbon nanotube shown in Fig. 3.

Group	$D_1$	$D_2$	$D_3$	$\sigma_D$	$v/u$	$\sigma_{v/u}$	% error
A	1916.633	1067.7	849.1	−0.167	0.0791	−0.0001	−0.18
B	1916.633	1088.7	827.6	0.333	0.0950	0.0003	0.31
C	1904.3	1200.2	701.1	3	0.1902	0.0030	1.57
D	1847.8	1416.2	434.1	−2.5	0.4320	−0.0034	−0.78
E	1799.3	1505.2	296	−1.9	0.5785	−0.0031	−0.53
F	1768.8	1548.3	218.5	2	0.6675	0.0036	0.53
G	1735.8	1595.3	143	−2.5	0.7754	−0.0050	−0.65
H	1706.8	1626.3	80	0.5	0.8649	0.0011	0.13

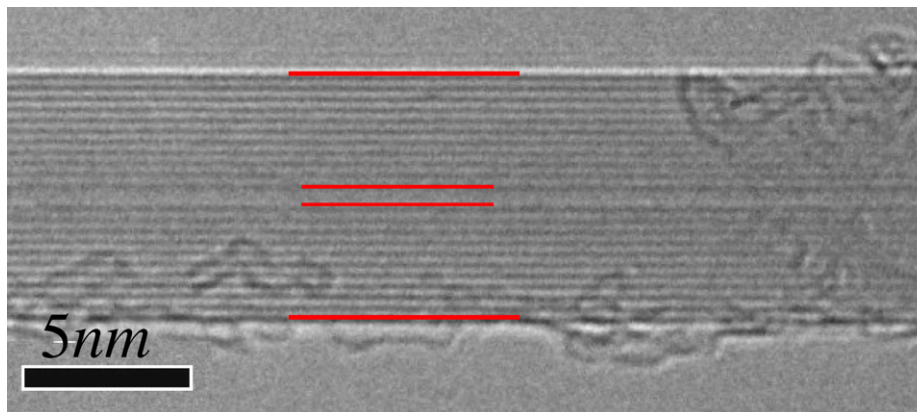
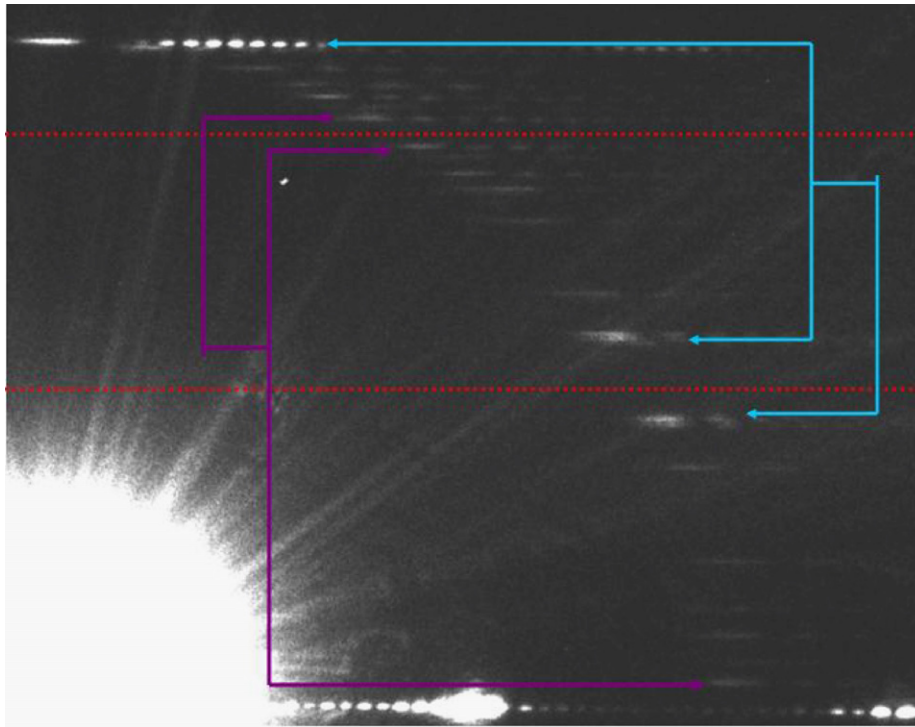


Fig. 3. High-resolution electron microscope image of an eleven-shell carbon nanotube with its innermost and the outermost shells are marked by red lines having diameter of 0.76 nm and 7.37 nm, respectively.



**Fig. 5.** An enlarged quadrant of the electron diffraction pattern shown in Fig. 4 with dotted red lines marking the zoning boundaries. There are seven layer lines in zone  $Z_1$ , eight in zone  $Z_2$  and eight in zone  $Z_3$ . Turquoise arrows show the grouping of the layer lines corresponding to shell A of the smallest helicity while the purple arrows mark the layer lines corresponding to shell H of the largest helicity. All other helicities between these two values are identified by grouping the corresponding layer lines from each zone in descending/ascending ( $L_1$  and  $L_3/L_2$ ) order in triplets.

smallest helicity present, which is formed by the first layer line in zone  $Z_1$  and zone  $Z_3$ , and the last layer line in zone  $Z_2$ . As the families of layer lines of higher helicities are grouped, the layer lines in the  $Z_1$  and  $Z_3$  zones in descending order and those in the  $Z_2$  zone in ascending order are matched accordingly, with the first line in zone  $Z_1$  being counted twice (see Fig. 5).

The uncertainty in the  $v/u$  ratios comes from the uncertainties in the measurement of layer line spacings  $D_1$  and  $D_2$ . This uncertainty can be expressed as

$$\sigma_{v/u} = \frac{3\sqrt{D_1^2 + D_2^2}\sigma_D}{(2D_1 - D_2)^2} \quad (3)$$

where  $\sigma_D = D_1 - (D_2 + D_3)$  represents the experimental error in the measurement of layer line spacings. Once all helicities are grouped and the approximate diameter of each shell is measured from the HRTEM images, the  $v/u$  ratios and their uncertainties are calculated as given in Table 1. Then, all possible chiral indices satisfying the measured  $v/u$  ratios within experimental errors are found by use of a computer script that facilitates this procedure more effectively. Table 2 gives the final assignment of the chiral indices of each and every shell of the eleven-shell carbon nanotube together with the inter-shell spacing  $d$  and metallicity (metallic ( $M$ ) or semi-conducting ( $S$ )).

To improve the accuracy of the deduced chiral indices, it is also very useful to examine and match the experimental and simulated intensity distribution on the equatorial line using the following equation:

$$I = |F(R, L = 0)|^2 = \left| f \sum_i^N d_i J_0(\pi R d_i) \right|^2 \quad (4)$$

where  $f$  is the atomic scattering factor for carbon atom,  $d_i$  the diameter of the  $i$ -th shell and  $N$  is the total number of shells [33].

**Table 2**

Final assignment of chiral indices ( $u, v$ ) for the eleven-shell carbon nanotube together with the diameter  $d$  and helicities calculated from the assigned chiral indices, the metallicity (metallic ( $M$ ) or semi-conducting ( $S$ )) of each shell and the index ratio  $v/u$  of assigned values ( $(v/u)_{assigned}$ ) and experimentally measured values ( $(v/u)_{exp}$ ). The last column gives the difference between the assigned and experimental index ratio  $v/u$ .

$u$	$v$	Metallicity	$d$ (nm)	Helicity ( $^\circ$ )	$(v/u)_{assigned}$	$(v/u)_{exp}$	% deviation
7	4	$M$	0.755	21.05	0.5714	0.5785	1.22
14	8	$M$	1.510	21.05	0.5714	0.5785	1.22
18	14	$S$	2.176	25.87	0.7778	0.7754	-0.31
22	19	$M$	2.783	27.58	0.8636	0.8649	0.15
42	4	$S$	3.456	4.50	0.0952	0.095	-0.25
50	4	$S$	4.081	3.81	0.0800	0.0791	-1.14
42	28	$S$	4.778	23.41	0.6667	0.6675	0.12
62	12	$S$	5.387	8.69	0.1935	0.1902	-1.76
56	32	$M$	6.041	21.05	0.5714	0.5785	1.22
63	36	$M$	6.796	21.05	0.5714	0.5785	1.22
74	32	$M$	7.374	17.11	0.4324	0.432	-0.10

Fig. 6 shows the simulated intensity distribution on the equatorial line using the assigned chiral indices given in Table 2 and the intensity distribution obtained from the experimental EDP. The peak positions and the overall shape of the curves agree well with each other, suggesting that the assignment of the chiral indices is the most plausible one.

## 5. Discussion

In general, for a chiral nanotube with missing layer lines in the EDP, the number of helicities can be found from the number of layer lines observed experimentally using a modular algorithm. For a modulo 3, the divisor gives the number of the distinct helicities if the remainder is zero though this does not have to be equal to the

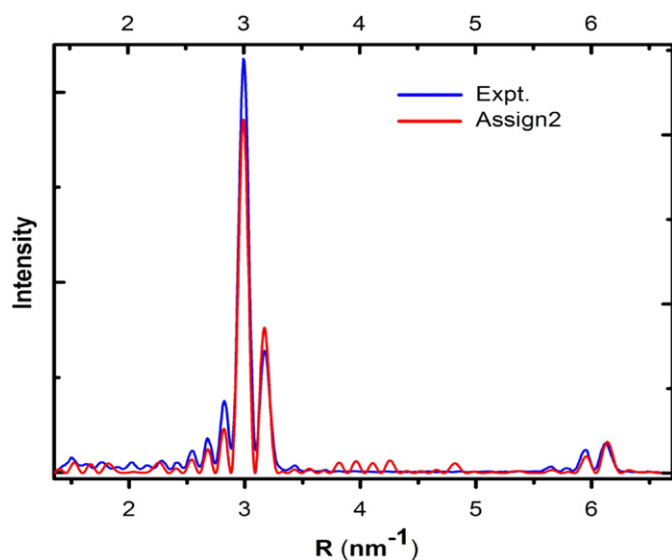


**Fig. 6.** Comparison of the experimental intensity distribution (blue) and simulated intensity distribution using the deduced chiral indices (red) on the equatorial line. The agreement for the positions and overall shape of the peaks are quite good. (For interpretation of the references to colour in this figure legend, the reader is referred to the web version of this article.)

number of shells in the carbon nanotube in case one helicity is shared by more than one shell. For the case of non-zero remainder, the divisor plus one gives the number of distinct helicities because the non-zero remainder indicates that some layer lines are in overlap with each other. Since the number of observed layer lines should be three times as many as the number of helicities, the difference of the expected and the observed number of principal layer lines gives the number of the layer lines in overlap with other layer lines. For our case, we have observed 23 distinct principal layer lines and this gives  $23=2 \pmod{3}$ . Therefore, we have eight different helicities present in the nanotube and shells of chiral indices (7,4), (14,8), (56,32) and (63,36) share the same helicity of  $21.05^\circ$ .

The reliability of the indexing procedure is largely dictated by the precision in the measurement of the layer lines in zone  $Z_1$  since this is the zone with the smallest width of  $0.154/a$  among all three zones. In the example given above, the groups of layer lines A and B in Table 1 corresponding to chiral angles of  $3.81^\circ$  and  $4.50^\circ$ , respectively, share a common layer line. According to their chiral indices (50,4) and (42,4), layer line  $L_1$  of group A and group B should be positioned at  $1.152/a$  and  $1.151/a$ , respectively. If we could measure experimentally this difference ( $0.001/a=0.0041 \text{ nm}^{-1}$ ) from the EDP, total 150 different helicities would be distinguished from zone  $Z_1$ . However, during the course of our study we have come across as many as five helicities sharing the same layer line  $L_1$  so a maximum uncertainty of  $0.006/a=0.0244 \text{ nm}^{-1}$  was present from the measured layer line positions. This resolution would allow a maximum of total 25 shells of different helicities to be resolved. On the other hand, when  $L_2$  and  $L_3$  layer lines can be used to identify each helicity, a larger number of shells than the aforementioned case can be characterized. However, the accuracy in the measurement of  $v/u$  ratios would be reduced greatly due to the use of smaller layer line spacings ( $D_2/D_3$ ). To overcome this hurdle, higher order layer lines such as  $L_4$  should be used to improve accuracy [29].

The multi-shell carbon nanotubes used in our study were grown by a dc arc-discharge in hydrogen gas [35]. Two important features that these nanotubes have are high-purity and a narrow channel in the center [36]. The diameter of the innermost shell is usually about 1.0 nm or less. In our case, it was a (7,4) carbon nanotube with a

diameter of 0.755 nm. The example studied here suggests that the structural orientation between the adjacent shells of carbon nanotubes is weak, as observed in the recent work on double-walled nanotubes [37]. Although the first two inner shells of the examined nanotube have commensurate structures, the structure of nanotubes in this MWNT sample in general has a random distribution. Considering the weak dependence of the formation energy of nanotubes on helicity [38], we believe that the interactions between the neighboring shells in a nanotube have little effect on the growth mechanism.

## 6. Conclusions

A systematic electron diffraction procedure has been developed to obtain the chirality of each and every shell in multi-shell carbon nanotubes. This method is based on the use of a zoning scheme to identify and group the principal layer lines corresponding to each helicity in an electron diffraction pattern and to measure the helicity and the ratio of the chiral indices  $v/u$  accurately from the layer line spacings. When this is combined with the diameter of each shell obtained from HRTEM images, the chiral indices of each and every shell of an eleven-shell carbon nanotube have been determined as an example of application. The selection of possible chiral indices using the measured index ratios  $v/u$  has also been automated to speed up the otherwise time-consuming process.

## Acknowledgements

The authors wish to thank Professors X. Zhao and Y. Ando for the carbon nanotube samples used in this study. This work is partially supported by NSF-ECCS 0725759 (LCQ).

## References

- [1] R. Saito, G. Dresselhaus, M.S. Dresselhaus, *Physical Properties of Carbon Nanotubes*, Imperial College Press, London, 1999.
- [2] N. Hamada, S. Sawada, A. Oshiyama, *Phys. Rev. Lett.* 68 (1992) 1579.
- [3] R. Saito, M. Fujita, G. Dresselhaus, M.S. Dresselhaus, *Appl. Phys. Lett.* 60 (1992) 2204.
- [4] A.M. Rao, E. Richter, S. Bandow, B. Chase, P.C. Eklund, K.A. Williams, S. Fang, K.R. Subbaswamy, M. Menon, A. Thess, R.E. Smalley, G. Dresselhaus, M.S. Dresselhaus, *Science* 275 (1997) 187.
- [5] A. Jorio, R. Saito, J.H. Hafner, C.M. Lieber, M. Hunter, T. McClure, G. Dresselhaus, M.S. Dresselhaus, *Phys. Rev. Lett.* 86 (2001) 1118.
- [6] C. Fantini, A. Jorio, M. Souza, M.S. Strano, M.S. Dresselhaus, M.A. Pimenta, *Phys. Rev. Lett.* 93 (2004) 147406.
- [7] S.M. Bachilo, M.S. Strano, C. Kittrell, R.H. Hauge, R.E. Smalley, R.B. Weisman, *Science* 298 (2002) 2361.
- [8] A. Hagen, T. Hertel, *Nano Letters* 3 (2003) 383.
- [9] J.W.G. Wildoer, L.C. Venema, A.G. Rinzler, R.E. Smalley, C. Dekker, *Nature* 391 (1998) 59.
- [10] T.W. Odom, J.L. Huang, P. Kim, C.M. Lieber, *Nature* 391 (1998) 62.
- [11] S. Iijima, *Nature* 354 (1991) 56.
- [12] L.-C. Qin, *J. Mater. Res.* 9 (1994) 2450.
- [13] A.A. Lucas, V. Bruyninckx, P. Lambin, *Europhys. Lett.* 35 (1996) 355.
- [14] L.-C. Qin, T. Ichihashi, S. Iijima, *Ultramicroscopy* 67 (1997) 181.
- [15] L.-C. Qin, S. Iijima, H. Kataura, Y. Maniwa, S. Suzuki, Y. Achiba, *Chem. Phys. Lett.* 268 (1997) 101.
- [16] P. Lambin, A.A. Lucas, *Phys. Rev. B* 56 (1997) 3571.
- [17] L.-C. Qin, *Chem. Phys. Lett.* 297 (1998) 23.
- [18] L.-C. Qin, *Mater. Charact.* 44 (2000) 407.
- [19] L. Henrard, A. Loiseau, C. Journet, P. Bernier, *Eur. Phys. J. B* 13 (2000) 661.
- [20] M. Kociak, K. Suenaga, K. Hirahara, Y. Saito, T. Nakahira, S. Iijima, *Phys. Rev. Lett.* 89 (2002) 155501.
- [21] M. Kociak, K. Hirahara, K. Suenaga, S. Iijima, *Eur. Phys. J. B* 32 (2003) 457.
- [22] J.M. Zuo, I. Vartanyants, M. Gao, R. Zhang, L.A. Nagahara, *Science* 300 (2003) 1419.
- [23] M. Gao, J.M. Zuo, R.D. Twisten, I. Petrov, L.A. Nagahara, R. Zhang, *Appl. Phys. Lett.* 82 (2003) 2703.
- [24] Z. Liu, Q. Zhang, L.-C. Qin, *Appl. Phys. Lett.* 86 (2005) 191903.
- [25] Z. Liu, L.-C. Qin, *Chem. Phys. Lett.* 408 (2005) 75.
- [26] Z. Liu, Q. Zhang, L.-C. Qin, *Phys. Rev. B* 71 (2005) 245413.
- [27] J.C. Meyer, M. Paillet, G.S. Duesberg, S. Roth, *Ultramicroscopy* 106 (2006) 176.

- [28] L.-C. Qin, Rep. Prog. Phys 69 (2006) 2761.  
[29] L.-C. Qin, Phys. Chem. Chem. Phys. 9 (2007) 31.  
[30] J.M. Zuo, T. Kim, A. Celik-Aktas, J. Tao, Z. Krist. 222 (2007) 625.  
[31] J. Zhang, J.M. Zuo, Carbon 47 (2009) 3515.  
[32] Z. Liu, L.-C. Qin, Chem. Phys. Lett. 400 (2004) 430.  
[33] B.W. Smith, D.E. Luzzi, J. Appl. Phys. 90 (2001) 3509.  
[34] Z. Liu, L.-C. Qin, Chem. Phys. Lett. 402 (2005) 202.  
[35] X. Zhao, M. Ohkohchi, M. Wang, S. Iijima, T. Ichihashi, Y. Ando, Carbon 35 (1997) 775.  
[36] L.-C. Qin, X. Zhao, K. Hirahara, Y. Miyamoto, Y. Ando, S. Iijima, Nature 408 (2000) 50.  
[37] K. Hirahara, M. Kociak, S. Bandow, T. Nakahira, K. Itoh, Y. Saito, S. Iijima, Phys. Rev. B 73 (2006) 195420.  
[38] C.H. Kiang, W.A. Goddard III, Phys. Rev. Lett. 76 (1996) 2515.